Research on Fatigue Damage and Crack Propagation of GH4133B Superalloy Used in Turbine Disk of Aero-engine

Rongguo Zhao[1,*], Dunhou Tan[1], Xiyan Luo[2], Hongchao Li[1], Junfei Li[1], Wei Li[1], Xuehui Liu[3]

[1] College of Civil Engineering and Mechanics, Xiangtan University, Xiangtan 411105, China
[2] College of Resources and Environmental Science, Chongqing University, Chongqing 401331, China
[3] Liyang Aero-Engine Corporation, Aviation Industry Corporation of China, Anshun 561102, China
* Corresponding author: zhaorongguo@163.com

Abstract The fatigue damage and fracture of GH4133B superalloy used in turbine disk of aero-engine are studied. Firstly, the fatigue limit is measured, and the relation between electric resistance change ratio and number of fatigue loading cycles is investigated for smooth samples. Then, the fatigue crack propagation tests are carried out at various stress ratios, and the fatigue crack propagation threshold values are measured for standard compact tension samples. The research results indicate that the theoretical fatigue limit agrees well with experimental one, the modified Chaboche model can predict the fatigue damage preciously, and the Paris formula considering fatigue threshold can describe the crack propagation behavior accurately. Finally, the crack propagation equations and loads are derived using the inverse deducing method based on the fractography of smaples. It is suggested that the inverse deduced equations can predict the crack propagation behavior, and the predict results can effectively prevent the occurrence of fatigue fracture.

Keywords Fatigue, Damage, Crack propagation, Fractrography, GH4133B superalloy

1. Introduction

In the fracture accidents of engineering components and structures, the fracture caused by fatigue accounted for about 70% to 80% of all the fracture accidents [1]. In the field of aviation industry, the damage tolerance design criterion has been introduced into the structural design of the aircraft and aero-engine, instead of the traditional minimum safe life design criterion [2, 3]. As far as the fatigue damage mechanism is concerned, from the point of view of damage mechanics, the process of crack growth in material from initiation to propagation to ultimate failure is a one of continuous damage evolution. The damage evolution equation is stated by the relationship between the change of damage variable and the number of loading cycles. Therefore, constructing a suitable damage evolution equation becomes a key issue of the damage tolerance design. Many damage theories for various metals and their alloys under different conditions had been devoloped, and these models were reviewed, and they were grouped into six categories: linear damage rules; nonlinear damage curve and two-stage linearization approaches; life curve modification methods; approaches based on crack growth concepts; continuum damage mechanics models; and energy-based theories [4]. In general, the elastic modulus, fatigue cycles, microhardness, interface shrinkage, as well as electric resistance, etc., can be used to describe the fatigue damage of material. For most of the metals and their alloys, the electric resistance change method can be adopted to charaterize the fatigue damage evolution, which has better accuracy and sensitivity [5–7].

Fatigue crack growth in metals and alloys is a process controlled by many variables, which includes both external factors such as temperature, frequency, loading rate, stress ratio, mean stress, and internal factors such as content, microstructure, and inclusion. GH4133B is a nickel-based superalloy. Such alloy is selected to manufacture components operated at high temperature, such as turbine disk of aero-engine, for its resistance to sensitization, adaquate high temperature tensile strength and creep resistance. Hu [8] investigated the creep-fatigue interaction and the effect of loading history on the creep-fatigue damage of GH4133B superalloy at 600ºC in three cases of loading as continuous cyclic loading (CF), prior fatigue followed by creep loading (F+C), and prior

creep followed by fatigue loading (C+F), and found that the creep-fatigue damage in the cases of CF and F+C was larger than unity, while that was smaller than unity at C+F. Luo [9] carried out a statistical analysis on the mechanical parameters of GH4133B superalloy at room temperature, and found that the three-parameter Weibull distribution was fit for the reliability assessment of this superalloy. Padula II [10] investigated the effect of grain size on high frequency fatigue crack propagation of nickel-based superalloys at various stress ratios. The results indicated that there is no effect of frequency on the fatigue behavior at ambient temperature. The threshold stress intensity for fatigue crack propagation decreases with decreasing grain size and with increasing stress ratio.
In this paper, the fatigue damage and fracture tests of GH4133B superalloy used in turbine disk of earo-engine are carried out at room temperature. The fatigue limit is measured for smooth samples at various stress amplitudes, and the fatigue crack growth rates are detected for standard compact tension samples under different stress ratios. A modified Chaboche model is applied to predict the accumulated damage of smooth samples of GH4133B superalloy at symmetrical cycle loading, and a Paris formula considering threshold stress intensity factor range is deduced to describe the fatigue crack growth behavior. The fracture surface morphologies of standard compact tension samples of GH4133B superalloy are investigated using scanning electron microscope, and the crack growth equations and loads are derived using the inverse deducing method.

2. Material and samples

The material used in this research is a nickel-based GH4133B superalloy with following chemical composition in % weight: C 0.06, Cr 19~22, Al 0.75~1.15, Ti 2.5~3.0, Fe 1.5, Nb 1.3~1.7, Mg 0.001~0.01, Zr 0.01~0.1, B 0.01, Ce 0.01, Mn 0.35, Si 0.65, P 0.015, S 0.007, Cu 0.07, Bi 0.0001, Sn 0.0012, Sb 0.0025, Pb 0.001, As 0.0025, and the balance nickel. The superalloy samples are machined from a turbine disk. The heat treatment process is as follows: 1080±10ºC, 8 hours, air cooling with 750ºC±10ºC, 16 hours air cooling. The samples for fatigue damage tests are machined in rod shape, as shown in Fig. 1. The samples for fatigue crack growth tests are machined in the shape of standard compact tension sample, as shown in Fig. 2.

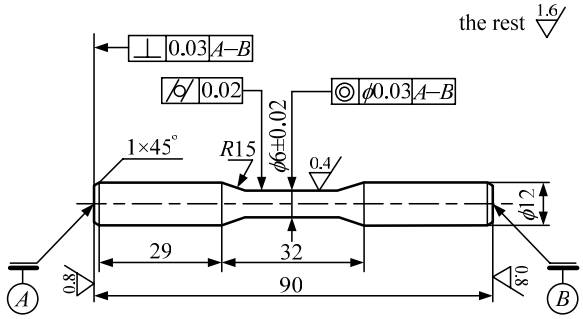

Figure 1. Dimensions of smooth sample (unit: mm)

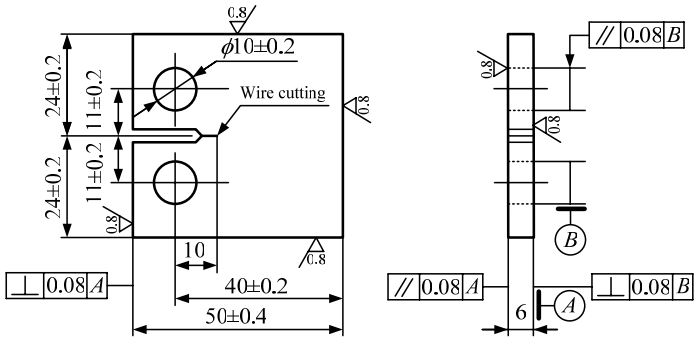

Figure 2. Dimensions of standard compact tension sample (unit: mm)

3. Fatigue life and fatigue damage analysis

3.1. Fatigue life test

At room temperature and atmospheric pressure, the fatigue tests for smooth samples of GH4133B superalloy are performed on a servo hydraulic test machine (CSS-280S-20) of ±20kN loading capacity. Under symmetrical cyclic loading condition (30 Hz sine wave, stress ratio R=–1), the fatigue life tests are carried out at various stress amplitudes. The fatigue limit is defined as 10^7 cycles. The stress amplitudes are assigned as 256MPa, 320MPa, 400MPa, 432MPa, 462MPa and 538MPa, respectively. In the case of stress amplitude as 256MPa or 538MPa, only one fatigue test for a smooth sample is carried out, while for the other stress amplitudes, four fatigue tests are performed for eight smooth samples of GH4133B superalloy. During the process of fatigue tests, a multi-parameter measurement mode is adopted, that is, except for recording the number of fatigue loading cycles, the values of electric resistance of smooth sample are measured every certain number of loading cycles by a QJ-57 type DC resistance bridge whose scale overs the range from 0.01μΩ to 1.1111kΩ, which is producted by Shanghai Sute Electrical Appliance Limited Company. Therefore, the accumulated fatigue damage for the sample of GH4133B superalloy during the fatigue process is monitored by measuring electric resistance change.

3.2. Fatigue life analysis

Using the up-down stress amplitude method, the fatigue life measured in the tests is determined as 288MPa, which is the mean value of stress amplitude 256MPa and 320MPa. The three-parameter power function expression is adopted to describe the fatigue S-N curve, that is

$$N_{\mathrm{f}} = \sigma_{\mathrm{f}}(\sigma_{\mathrm{a}} - \sigma_{\mathrm{ac}})^{-m}, \tag{1}$$

where, N_{f} is fatigue life, σ_{f}, σ_{a} and m are undetermined coefficients, and σ_{ac} is theoretical fatigue limit. Usually, the value m is obtained as 2 to 4. In this work, the value m is set as 2. Taking logarithm on both sides of above equation, and the equation can be rewritten as

$$\lg N_{\mathrm{f}} = \lg \sigma_{\mathrm{f}} - 2\lg(\sigma_{\mathrm{a}} - \sigma_{\mathrm{ac}}), \tag{2}$$

Eq. (2) shows a linear relationship between logarithmic fatigue life $\lg N_{\mathrm{f}}$ and $\lg(\sigma_{\mathrm{a}}-\sigma_{\mathrm{ac}})$, and the slope is 2. According to the experimental data obtained from the fatigue life tests, using a standard normal distribution function to calculate the values of fatigue life at survival probabilities as 50%, 90%, 95% at various stress amplitudes, the P-S-N equations at survival probabilities as 50%, 90% and 95% are individually achieved by using nonlinear regression method as

$$N_{\mathrm{f}} = 2.987\times10^{10}(\sigma_{\mathrm{a}} - 233.43389)^{-2}, \tag{3}$$

$$N_{\mathrm{f}} = 2.008\times10^{10}(\sigma_{\mathrm{a}} - 229.50659)^{-2}, \tag{4}$$

$$N_{\mathrm{f}} = 1.795\times10^{10}(\sigma_{\mathrm{a}} - 228.36174)^{-2}, \tag{5}$$

It can be seen that the theoretical fatigue limit σ_{ac} in Eq. (1) is calculated as 233.43389MPa, and the experimental one is measured as 288MPa, the relative error is about 18.95%. According to Eq. (3), Eq. (4) and Eq. (5), the P-S-N curves at survival probabilities as 50%, 90% and 95% are individually plotted, and are compared with the estimated values of fatigue life, as shown in Fig. 3. It can be found from Fig. 3 that the theoretical P-S-N curve is well fitted with the estimated values of fatigue life at survival probability as 50%, while at survival probabilities as 90% and 95%, there are some difference between the theoretical curves and the estimated values.

3.3. Fatigue damage analysis

As aforementioned above, during the process of fatigue life tests, the multi-parameter measurement

mode is applied to measure the electric resistance of GH4133B superalloy samples every certain numerber of loading cycles at various stress amplitudes. According to the definition of damage variable, the damage variable D charaterized by electric resistance can be written as

$$D = 1 - \frac{R_0}{R}, \text{ or } D = \frac{\Delta R}{R_0 + \Delta R}, \tag{6}$$

where, R_0 is the electric resistance before damage, R is the electric resistance after damage, and ΔR is the difference between R and R_0, which is called as electric resistance change. In this work, a modified Chaboche damage model is derived to describe the damage evolution, that is

$$D = 1 - \left(1 - \frac{N}{N_f}\right)^{1/(1+\beta_1(\sigma_a)+\beta)}, \tag{7}$$

Substituting Eq. (6) into Eq. (7), the fatigue damage evolution equation characterized by electric resistance change can be written as

$$\frac{\Delta R}{R_0} = \left(1 - \frac{N}{N_f}\right)^{-1/(1+\beta_1(\sigma_a)+\beta} - 1, \tag{8}$$

where, N is the number of fatigue loading cycles, N_f is the fatigue life, β and β_1 are the fatigue parameters, and the parameter β_1 is the function of the stress amplitude σ_a.

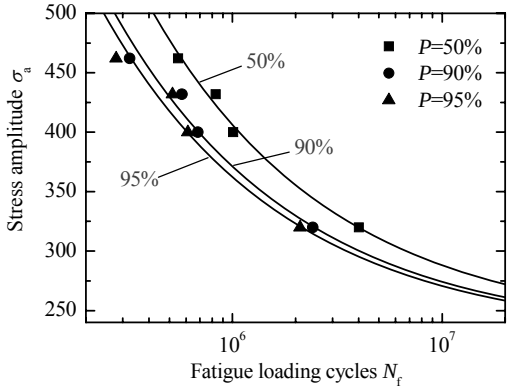

Figure 3. *P-S-N* curves at different survival probabilities

According to Eq. (8), the theoretical damage evolution equations at various stress amplitudes are derived using the nonlinear regression analysis of experiment data obtained in the electric resistance tests. Corresponding to stress amplitudes applied as 320MPa, 400MPa, 432MPa and 462MPa, the values of damage parameter $1+\beta+\beta_1(\sigma_a)$ are determined as 26.543, 31.571, 40.177 and 46.822, respectively. The comparisons between theoretical fatigue damage evolution curves and test data are shown in Fig. 4. Corresponding to the various stress amplitudes, the accumulated fatigue damages of two samples in each group are collected. In Fig. 4, the square symbols denote the test date obtained from the first sample, while the circle symbols denote the test data obtained from the second sample of each group, and the solid lines represent the theoretical results. It can be found from Fig. 4 that the theoretical predicted values are in good agreement with the experimental data, which indicates that the electric resistance change ratio under cyclic loading can be used to describe the process of fatigue damage evolution of GH4133B superalloy.

In the fatigue nucleation and small crack propagation stage (stage I), the fatigue damage is mainly dominated by a process of microdamge nucleation. Furthermore, due to the tension-pressure mode of cyclic loading, the action of compressive stress results in some small crack interfaces colsed, leading to the corresponding electric resistance change smaller, which can be reflected from Fig. 4(a) to (d), that is, the damage increases slowly with number of cycle in the early part of damage evolution curve. With the propagation and coalescence of small cracks, the damage degree becomes

larger, following with increasing electric resistance, and the electric resistance change ratio transits from a relatively flat stage to an acceleration stage, which is called stable fatigue crack propagation stage (stage II). With increasing number of loading cycles, the fatigue propagation moves from a stable stage to an acceleration stage (stage III), and finally leads to fracture failure. In this stage, the damage change rates very large, and the corresponding electric resistance change ratios are also large, as shown in the last parts of fatigue damage evolution curves.

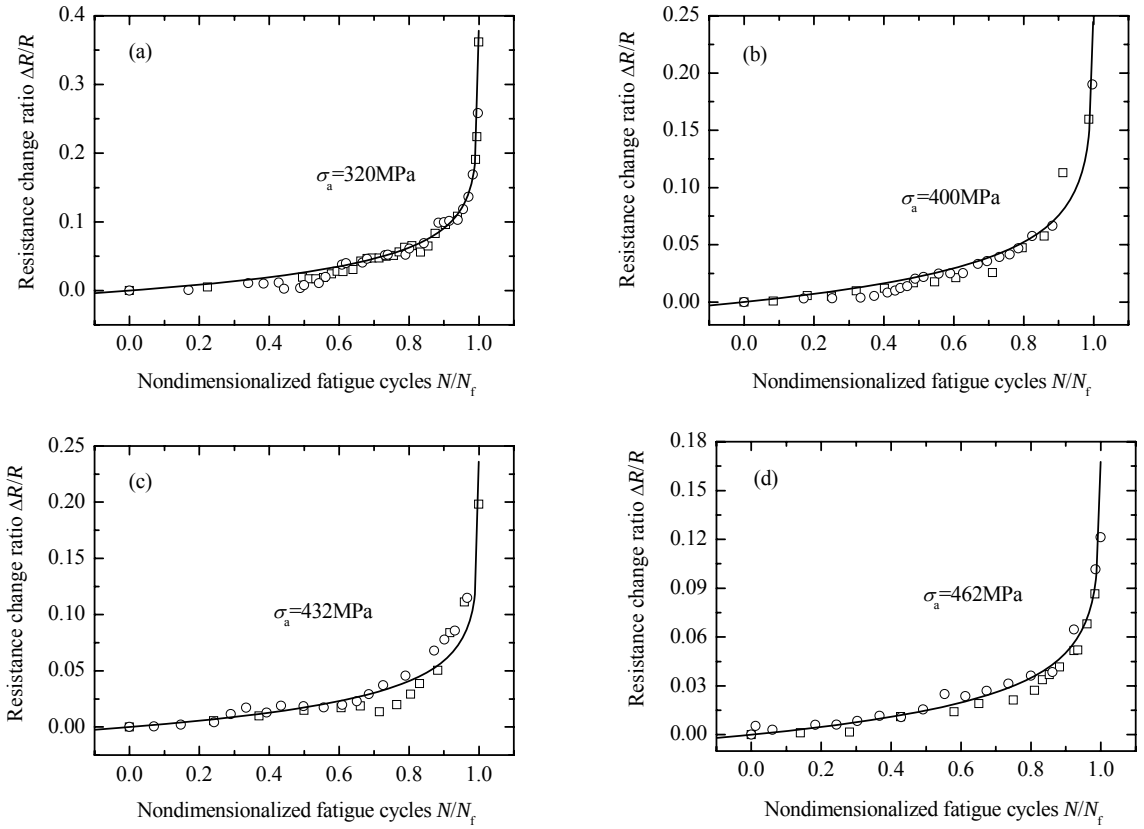

Figure 4. Fatigue damage evolution curves at various stress amplitudes

As aforementioned above, when the stress amplitude σ_a increases from 320MPa to 462MPa, the value of parameter $1+\beta+\beta_1(\sigma_a)$ increases from 26.543 to 46.882. However, the chang rate of electric resistance change ratio is reversed with increasing stress amplitude, which indicates that when the stress amplitude becomes higher, to achieve the same degree of damage as that at lower one, the proportion of consumed fatigue life over the total fatigue life will increase. That is, in the fatigue tests, as the stress amplitude increases, the proportion of fatigue life in the stage II and stage III of crack propagation will decrease, and the total fatigue life is mainly consumed in the stage I of fatigue crack initiation and small crack propagation. Therefore, the change rate of electric resistance change ratio is also relatively slow.

4. Fatigue crack propagation behavior and fractography reverse model

4.1. Fatigue crack propagation tests

The fatigue crack propagation tests for standard compact tension samples of GH4133B superalloy are performed on the CSS-280S-20 test machine. Under cyclic loading conditions (6Hz sine wave, stress ratio R=0.02, 0.1, 0.2, 0.4), the fatigue crack propagation tests are carried out. According to the different values of stress ratio, the tests are categorized as four groups, and two samples prepare

for each group. The approach of specified number of fatigue loading cycles is applied to determine the threshold stress intensity factor range ΔK_{th}, and an EVO scanning electron microscope is applied to investigate the fracture surface morphologies of samples of GH4133B superalloy.

4.2. Fatigue crack propagation behavior

As the stress ratio R=0.02, 0.1, 0.2 and 0.4, the threshold stress intensity factor ranges ΔK_{th} measured in the tests are 11.842MPa·m$^{1/2}$, 11.313MPa·m$^{1/2}$, 9.773MPa·m$^{1/2}$ and 7.440MPa·m$^{1/2}$, respectively. The relationship between the crack propagation rate da/dN and stress intensity factor range ΔK is shown in Fig. 5(a). It can be found from Fig. 5(a) that the crack propagation rate da/dN increases with increasing stress intensity factor range ΔK, and with increasing stress ratio. However, under the condition of low stress intensity factor ranges, the differences among the experimental data of crack propagation rate at different stress ratios are very small, which indicates that the effect of stress ratio on fatigue crack propagation rate are weak at low stress intensity factor ranges.

The Paris formula is applied to carry out a regression analysis for experimental data of fatigue crack propagation at various stress ratios. The Paris formula is written as

$$\frac{\mathrm{d}a}{\mathrm{d}N} = C(\Delta K)^m, \tag{9}$$

where, a is crack length, N is number of fatigue loading cycles, C and m are parameters determined by the crack propagation tests. Taking logarithm both sides of Eq. (9), Eq. (9) can be rewritten as

$$\lg\left(\frac{\mathrm{d}a}{\mathrm{d}N}\right) = \lg C + m\lg(\Delta K), \tag{10}$$

It can be seen from Eq. (10) that the relationship between crack propagation rate da/dN and stress intensity factor range ΔK shows a linear one in double-logrithmic coordinates, and the slope and intercept are individually m and lg$C$. At stress ratio R=0.02, 0.1, 0.2 and 0.4, the experimental data of fatigue crack propagation are analyzed by Eq. (10) using the least square regression method, and the crack propagation rate equations are individually derived as

$$\lg\left(\frac{\mathrm{d}a}{\mathrm{d}N}\right) = -8.229 + 2.700\times\lg(\Delta K), \tag{11}$$

$$\lg\left(\frac{\mathrm{d}a}{\mathrm{d}N}\right) = -8.403 + 2.858\times\lg(\Delta K), \tag{12}$$

$$\lg\left(\frac{\mathrm{d}a}{\mathrm{d}N}\right) = -8.807 + 3.171\times\lg(\Delta K), \tag{13}$$

$$\lg\left(\frac{\mathrm{d}a}{\mathrm{d}N}\right) = -8.587 + 3.176\times\lg(\Delta K), \tag{14}$$

According to Eq. (11), Eq. (12), Eq. (13) and Eq. (14), the theoretical curves of crack propagation rate versus stress intensity factor range are plotted, as shown the solid lines in Fig. 5(a). It can be found from Fig. 5(a) that the theoretical results are in good agreement with the experimental data, and the value of slope m increases monotonously from 2.700 to 3.176 with increasing stress ratio from 0.02 to 0.4, indicating that the crack propagation rate increases with increasing stress ratio, which is consistent with the aforementioned experiment results. Therefore, the Paris formula can be used to describe the fatigue crack propagation behavior of GH4133B superalloy.

Intending to describe the crack propagation behavior in the fatigue tests of GH4133B superalloy at any stress ratio more precisely, a threshold stress intensity factor range ΔK_{th} is introduced into Eq. (9), and the Paris formula is modified as

$$\frac{\mathrm{d}a}{\mathrm{d}N} = B(\Delta K - \Delta K_{th})^n, \tag{15}$$

where, B and n are material parameters determined by the fatigue crack propagation tests. Taking logarithm both sides of Eq. (15), Eq. (15) can be rewritten as

$$\lg\left(\frac{\mathrm{d}a}{\mathrm{d}N}\right) = \lg B + n\lg(\Delta K - \Delta K_{\mathrm{th}}), \tag{16}$$

It can be found from Eq. (16) that the relation between logrithmic crack propagation rate lg(da/dN) and lg(ΔK–ΔK_{th}) shows a linear one, and the slope and intercept are individually m and lg$B$. As aforementioned above, in the cases of stress ratio R=0.02, 0.1, 0.2 and 0.4, the threshold stress intensity factor ranges (ΔK_{th}) measured in the tests are 11.842, 11.313, 9.773 and 7.440MPa·m$^{1/2}$, respectively. The linear regression analysis on the experiment data is performed by using Eq. (16), and the crack propagation rate equations considering ΔK_{th} are individually derived as

$$\lg\left(\frac{\mathrm{d}a}{\mathrm{d}N}\right) = -6.858 + 2.055\times\lg(\Delta K - 11.842), \tag{17}$$

$$\lg\left(\frac{\mathrm{d}a}{\mathrm{d}N}\right) = -6.994 + 2.192\times\lg(\Delta K - 11.313), \tag{18}$$

$$\lg\left(\frac{\mathrm{d}a}{\mathrm{d}N}\right) = -7.326 + 2.457\times\lg(\Delta K - 9.773), \tag{19}$$

$$\lg\left(\frac{\mathrm{d}a}{\mathrm{d}N}\right) = -7.376 + 2.571\times\lg(\Delta K - 7.440), \tag{20}$$

Considering the threshold stress intensity factor range ΔK_{th}, and in double-logrithmic coordinates, the theoretical curves of crack propagation rate da/dN versus stress intensity factor rang ΔK are plotted by using Eq. (17), Eq. (18), Eq. (19) and Eq. (20), as shown the solid lines in Fig. 5(b).

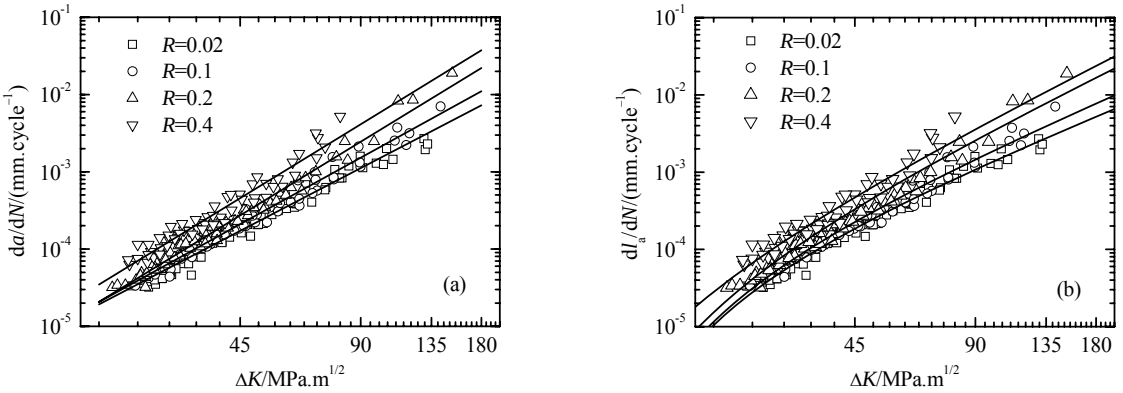

Figure 5. Curves of crack propagation rate: (a) by Paris formula; (b) by modified Paris formula

It can be found from Fig. 5(b) that the theoretical results are well fitted with test data, especially in the case of small values of stress intensity factor range ΔK, comparing with Eq. (11) to Eq. (14), the precise theoretical results are obtained by using Eq. (17) to (20), which can be seen from the comparison between theoretical curve and experimental data in Fig. 5 and Fig. 6. Therefore, the modified Paris formula can not only be used to predict the value of threshold stress intensity factor at different stress ratio, but also can describe the fatigue crack propagation behavior accurately.

4.3. Fractography reverse model

As aforementioned above, the fracture surface morphologies of standard compact tension samples of GH4133B superalloy are investigated using an EVO scanning electron microscope, and a series of fatigue striations are found in the crack steady propagation region. According to these fatigue striations on the fracture surface, the crack propagation rate equations and loads are derived using

the inverse educing method. For mode I crack, the expression of stress intensity factor range ΔK is

$$\Delta K = Y\Delta\sigma\sqrt{\pi a}\,, \tag{21}$$

where, $\Delta\sigma$ is external stress range, a is crack dimension parameter, Y is shape factor which relates to structure shape, crack location and dimension as well as load condition. Substituting Eq. (9) into Eq. (21), the expression of external stress range $\Delta\sigma$ is derived as

$$\Delta\sigma = \frac{1}{Y\sqrt{\pi a}}\left(\frac{1}{C}\cdot\frac{\mathrm{d}a}{\mathrm{d}N}\right)^{1/m}, \tag{22}$$

It can be found from Eq. (22) that if the values of crack propagation rate are measured, then the external stress range acted on the sample can be calculated using the inverse educing method. For standard compact tension sample (Fig. 2), the expression of stress intensity factor range ΔK is

$$\Delta K = \frac{\Delta P}{B\sqrt{W}}F(\alpha),\quad F(\alpha) = \frac{2+\alpha}{(1-\alpha)^{3/2}}\times(0.886+4.46\alpha-13.32\alpha^2+14.72\alpha^3-5.6\alpha^4), \tag{23}$$

where, ΔP is external load range, B is thickness, W is width, and α is the ratio of crack length a to width W. Substituting Eq. (9) into Eq. (22), the expression of external load range ΔP is derived as

$$\Delta P = B\sqrt{W}\left(\frac{1}{C}\cdot\frac{\mathrm{d}a}{\mathrm{d}N}\right)^{1/m}\Big/F(\alpha), \tag{24}$$

For example, in the case of R=0.4, the fracture surface morpologies in the steady propagation region at various stress intensity factors are shown in Fig. 6. Measuring the widths of damage striations on the fracture surface, and recording the corresponding number of loading cycles, thus the crack propagation rates are calculated. Using Eq. (23) and Eq. (24), the stress intensity factor ranges and external loads relating with crack propagation rates are derived.

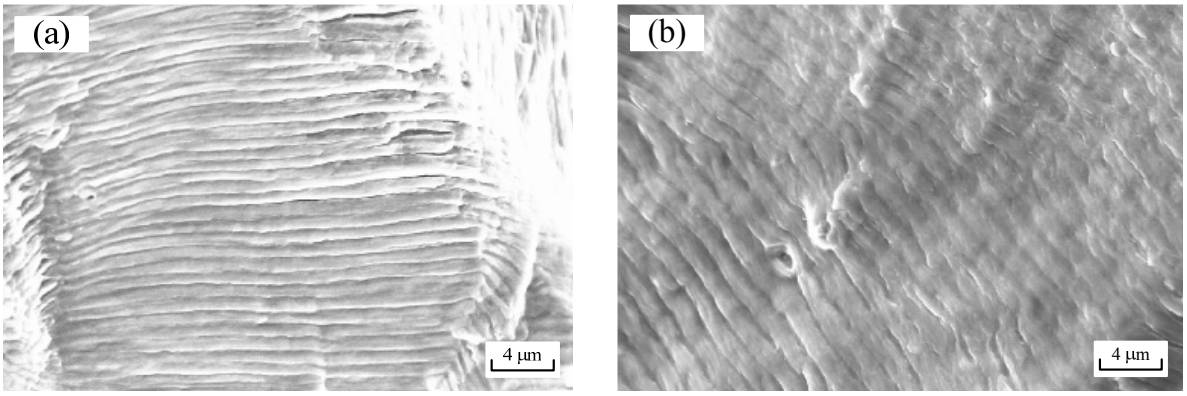

Figure 6. Fracture surface morpology: (a) ΔK=60.69MPa·m$^{1/2}$; (b) ΔK=80.53MPa·m$^{1/2}$

According to Eq. (16), the regression analysis on the calculated data obtained from the fractography is performed, and the inverse deduced equations on fatigue crack propagation are derived. In the cases of stress ratio R=0.02, 0.1, 0.2, 0.4, the inverse deduced equations are individually as

$$\lg\left(\frac{\mathrm{d}a}{\mathrm{d}N}\right) = -7.633+2.619\times\lg(\Delta K-11.842), \tag{25}$$

$$\lg\left(\frac{\mathrm{d}a}{\mathrm{d}N}\right) = -7.544+2.498\times\lg(\Delta K-11.313), \tag{26}$$

$$\lg\left(\frac{\mathrm{d}a}{\mathrm{d}N}\right) = -7.595+2.500\times\lg(\Delta K-9.773), \tag{27}$$

$$\lg\left(\frac{\mathrm{d}a}{\mathrm{d}N}\right) = -8.003+2.647\times\lg(\Delta K-7.440), \tag{28}$$

The comparison between the theoretical curves predicted by inverse deduced equations and analysis data obtain from the fractography is shown in Fig. 7. It can be seen from Fig. 7 that the theoretical curves are well fitted with analysis data, which indicates that the inverse deduced equations can be used to accuratelly describe the crack propagation behavior in the steady propagation region.

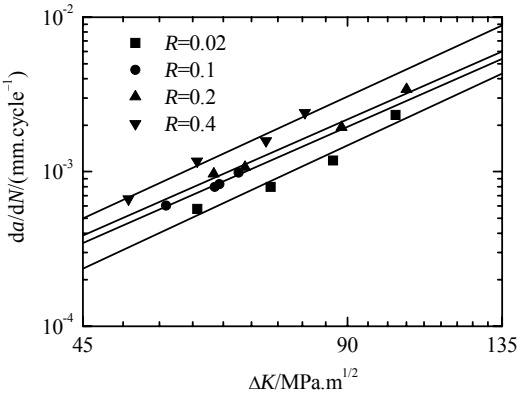

Figure 7. Inverse deduced curves of crack propagation rate

Following, these inverse deduced equations (from Eq. (25) to Eq. (28)) are generalized to describe the whole process of fatigue crack propagation. At various stress ratios, the comparisons between theoretical curves of fatigue crack propagation rate and experimental data are shown in Fig. 8.

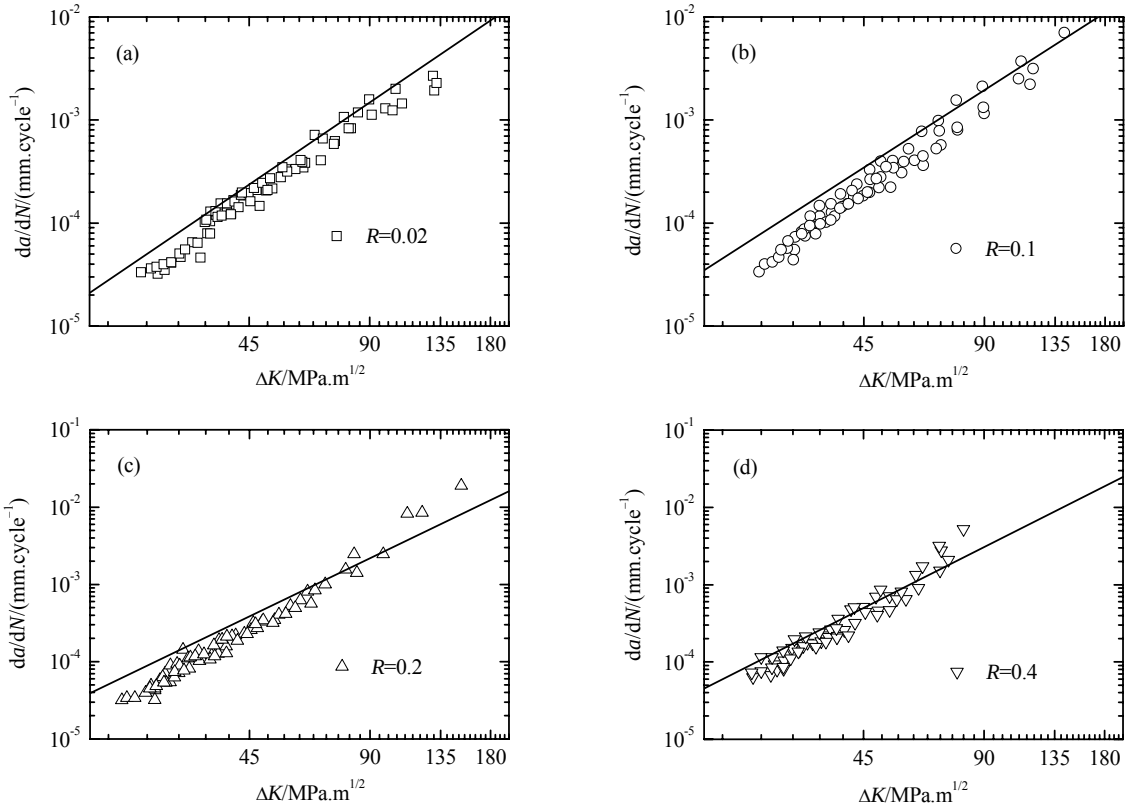

Figure 8. Crack propagation rate curves obtained by inverse deduced equations

It can be seen from Fig. 8 that the theoretical curves are basically consistent with experimental data, indicating that the inverse deduced equations derived from the analysis data obtained by measuring damage striations in steady propagation region of fracture surface, can still be used to predict the whole process of fatigue crack propagation. Furthermore, it can be found that if only the stress

intensity factor range ΔK is not too large, in other words, if only the fatigue crack is not at the later stage of accelerated growth region, the theoretical values are totally larger than that of experimental data, so the predicted results obtained by the inverse deduced equations tend to security.

5. Conclusions

(1) The fatigue life of GH4133B superalloy is measured, and the theoretical fatigue life is calculated, and the *P-S-N* curves at various survival probabilities are obtained. It is found that the theoretical fatigue limit agrees well with experimental one, and the fatigue life of GH4133B superalloy can accurately be estimated by the *P-S-N* curves.
(2) The modified Chaboche model can predict the accumulated damage of GH4133B superalloy preciously. Higher stress amplitude will result in a higher proportion of the fatigue life in stage I of fatigue crack initiation and small crack propagation to the total fatigue life, which is unfavorable to monitor the accumulative fatigue damage and to prevent fatigue fracture in the components.
(3) A modified Paris formula is achieved by introducing a threshold stress intensity factor range. The comparison between theoretical curves and experiment data shows that the modified Paris formula can not only be used to predict the value of threshold stress intensity factor range at different stress ratio, but also can describe the fatigue crack propagation behavior accurately.
(4) Based on the measurement data of fatigue striations and the modified Paris formula, the crack propagation rate equations and external loads are inversely deduced and calculated. It is found that the inverse deduced equations based on the fractography inverse model can predict the fatigue crack propagation behavior, and the predicted results tend to security.

Acknowledgements

The authors gratefully acknowledge the finanicial support of the Research Foundation of Education Burean of Hunan Province, China (No. 11B125).

References

[1] Q.P. Zhang, Z. Zhang, H.S. Wu, S.Z. Zuo. Physical and mathematical models of fatigue propagation and final rupture regions for metallic materials. Acta Aeronautica and Astronautica Sinica, 21(s), (2000) s11–s14. (in Chinese)
[2] E.J. Xu.The Effect of defects, damage and micro crack on total life and reliability of aeroengine components in service. Aeroengine, 29(2), (2003) 11–15. (in Chinese)
[3] J. Schijves. Fatigue damage in aircraft structures, not wanted, but tolerated? Int. J. Fatigue, 31(6), (2009) 998–1011.
[4] A. Fatemi, L. Yang. Cumulative fatigue damage and life prediction theories: A survey of the state of the art for homogeneous materials. Int. J. Fatigue, 20(1), (1998) 9–34.
[5] P. Starke, F. Walther, D. Eifler. New fatigue life calculation method for quenched and tempered steel SAE 4140. Materials Science and Engineering A, 523(1–2), (2009) 246–252.
[6] B. Sun, Y. Guo. High-cycle fatigue damage measurement based on electrical resistance change considering variable electrical resistivity. Int. J. Fatigue, 26(5), (2004) 457–462.
[7] D. Huang, P. C. Xu, Y.M. GUO. A research on the estimation of remaining service life for metals in fatigue. Journal of Experimental Mechanics, 18(1), (2003) 113–117. (in Chinese)
[8] D.Y. Hu, R.Q. Wang. Experimental study on creep-fatigue interaction behavior of GH4133B superalloy. Materials Science and Engineering: A, 515(1–2), (2009) 183–189.
[9] X.Y. Luo, R.G. Zhao, Y.Z. Jiang, H.C. Li, X.J. Li, X.H. Liu. Statistical analysis on mechanical properties of GH4133B superalloy used in turbine disk of aero-engine at ambient temperature. Chinese Journal of Mechanical Engineering, 46(22), (2010) 75–83. (in Chinese)
[10] S.A. Padula II, A. Shyam, R.O. Ritchie, W.W. Milligun. High frequency fatigue crack propagation behavior of a nickel-base turbine disk alloy. Int. J. Fatigue, 21(7), (1999) 725–731.